Journal of Solid State Chemistry 182 (2009) 1222–1228

Contents lists available at ScienceDirect

Journal of Solid State Chemistry

journal homepage: www.elsevier.com/locate/jssc

Structure of δ-Bi_2O_3 from density functional theory: A systematic crystallographic analysis

Dilpuneet S. Aidhy, Susan B. Sinnott, Eric D. Wachsman, Simon R. Phillpot, Juan C. Nino *

Department of Materials Science and Engineering, Rhines Hall, Gainesville, FL 32611, USA

ARTICLE INFO

Article history:
Received 2 October 2008
Received in revised form
29 January 2009
Accepted 7 February 2009
Available online 23 February 2009

Keywords:
Density functional theory
SOFC electrolyte
Crystallography
Ordering of vacancies

ABSTRACT

A systematic crystallographic analysis of the ⟨110⟩ and ⟨111⟩ vacancy-ordered structure of cubic δ-Bi_2O_3 obtained from electronic-structure calculations is presented. The ordering of vacancies leads to a doubling of the unit-cell that results in a $2\times2\times2$ fluorite super-structure, with an associated reduction in its space group symmetry from $Fm\bar{3}m$ to $Fm\bar{3}$. The Bi atoms present inside the ⟨111⟩ vacancy-ordered oxygen sublattice have equal Bi–O bond lengths, whereas, those present inside the ⟨110⟩ vacancy-ordered oxygen sublattice have three different pairs of Bi–O bond lengths. The specific ionic displacements and electronic charge configurations also depend on the nature of vacancy ordering in the oxygen sub-lattice.

1. Introduction

Pure and doped δ-Bi_2O_3 have the highest ionic conductivities known among fluorite structured materials, which also include yttria stabilized zirconia (YSZ) and doped ceria [1,2]. Doped δ-Bi_2O_3 is thus a candidate material for a bi-layer electrolyte in solid oxide fuel cells (SOFC), oxygen separation membranes and sensors operating at intermediate temperatures (400–600 °C). Cubic δ-Bi_2O_3 is a high temperature phase; to stabilize it at lower temperatures it is normally doped with lanthanide oxides. The addition of these dopants results in an ionic conductivity which decreases significantly [3] under prolonged aging, an effect that is attributed to the ordering of the unoccupied oxygen sites (vacancies) that are inherently present in δ-Bi_2O_3. It is believed that this vacancy ordering is due to either the different dopant radii or ionic polarizabilities or a combination of both [4]. Since, it is impossible to separate the effect of these two parameters experimentally, we have earlier used molecular-dynamics (MD) simulation to show that the ionic polarizability of the cations is in fact the most important factor in maintaining high conductivity by not allowing ordering of the oxygen vacancies [5]. In particular, the high ionic polarizability of bismuth allows easier oxygen diffusion. However, the lanthanides used as dopants have low ionic polarizability in comparison to bismuth, thereby enabling the development of the ordered defect structures. In this work, we have use density functional theory (DFT) to understand the atomistic and electronic environments that are associated with such an ordered structure. We also present a systematic crystallographic analysis of the vacancy-ordered structure of pure δ-Bi_2O_3 in terms of its space group, the effect of the ordering on the Bi–O bond lengths, the consequent ionic displacement and structural distortion in the sub-structures [5].

2. Methodology

We have performed standard DFT calculations using the Vienna *Ab initio* Simulation Package (VASP) package [6–8] within the generalized gradient approximation (GGA) exchange-correlation functional in the PW91 form [9]. The projector augmented wave (PAW) method [10] was applied to the core electrons (Bi [Xe]$4f^{14}5d^{10}$) and O[He]). A Monkhorst-Pack k-points grid of $6\times6\times6$ for systems containing $1\times1\times1$ non-cubic unit cells and $3\times3\times3$ k-points grid for $2\times2\times2$ systems was used with a plane wave cut-off of 500 eV. The positions of the ions were optimized such that the force on each ion was converged to better than 0.0005 eV/Å. Periodic boundary conditions were applied in all three spatial directions.

3. Structure of vacancy-ordered system

3.1. Space group analysis

The δ-phase of Bi_2O_3 forms in a fluorite-like structure. Properly speaking, the unoccupied anion sites in the fluorite lattice are not

* Corresponding author. Tel.: +1 (352) 846 3787; fax: +1 (352) 352 846 3355.
E-mail address: jnino@mse.ufl.edu (J.C. Nino).
URL: http://nino.mse.ufl.edu (J.C. Nino).

0022-4596/$ - see front matter © 2009 Elsevier Inc. All rights reserved.
doi:10.1016/j.jssc.2009.02.019

vacancies since they do not affect the anion to cation ratio. Rather, they are crystallographically allowed sites that remain unoccupied. However, these unoccupied anion sites are routinely referred to as vacancies because in the fluorite structure, one would expect a 1:2 ratio between cations and anions; thus the 2:3 ratio can be seen as an anion deficiency. Therefore, for simplicity and clarity, here we refer to these empty sites as vacancies. In agreement with experiments, the DFT simulations predict a defect-derivative fluorite crystal structure with ordering in the unoccupied anion sites in the ⟨110⟩ and ⟨111⟩ directions.

The space group of an ideal fluorite structure is $Fm\bar{3}m$ (225). In δ-Bi_2O_3, the overall cubic symmetry is maintained. However, the lattice parameter is very close to twice that of fluorite structures: 11.19761 Å as determined from the DFT calculations. The unit cell contains 16 Bi_2O_3 stoichiometric units rather than two as in the fluorite unit cell. The experimentally reported lattice parameter of a unit-cell of δ-Bi_2O_3 is 5.644 Å [11], which corresponds to 11.288 Å for the $2\times2\times2$ superstructure. This DFT error of 0.8% may be taken as representative of the degree of quantitative accuracy that can be expected in the analyses below. The superstructure lowers the symmetry to space group of $Fm\bar{3}$ (202). It is important to recall that $Fm\bar{3}$ is a maximal non-isomorphic t-subgroup of $Fm\bar{3}m$, where all translational symmetry is maintained but the order of the point group is reduced (from 48 to 24) [12]. In essence the $Fm\bar{3}$ is derived from the $Fm\bar{3}m$ in that the 4-fold rotation along ⟨100⟩ is reduced to a 2-fold rotation, and that the 2-fold rotation along ⟨110⟩ and the associated perpendicular mirror planes are lost. The resulting space group parameters of the δ-Bi_2O_3 are presented in Table 1. The reduction in the 4-fold rotation to 2-fold rotation is due to the displacement of the Bi ions in ⟨100⟩. However, this loss in symmetry is neither a consequence of the vacancies nor their ordering. The relative displacement of Bi ions has been shown elsewhere [5, Fig. 12] and is further discussed below.

This superstructure contains three crystallographically distinct Bi sites, Bi(1) at 4*a*, Bi(2) at 4*b* and Bi(3) at 48 h, and two crystallographically distinct O sites, O(1) and O(2), both at 96*i*. Taking the occupancy into account, the superstructure is comprised of 32 cations and 48 anions, i.e., 16 formula-units per unit cell ($Z=16$). In the case of the cation, there are two different sites each of multiplicity four, Bi(1) and Bi(2), and one site of multiplicity 48, Bi(3). The occupancy of Bi(1) and Bi(2) sites is 1.0 and of Bi(3) is 0.5.

There are thus 64 anion sites available in the structure, of which 48 are occupied by oxygen ions equally distributed on the two crystallographically different sites, O(1) and O(2); the remaining 16 sites are unoccupied (vacancies). The crystallographic sites of 1/8 of the superstructure are represented in Fig. 1. A layered sequence of the eight sub unit-cells of the complete $2\times2\times2$ cubic superstructure has been shown previously [5]. As reference points, the conventional oxygen fluorite positions (8*c* in ideal fluorite) are shown in black in Fig. 1; however, these points do not correspond to ion positions in the superstructure. Each of these fluorite oxygen positions is surrounded by three O(1) or O(2) sites, only one of which is occupied at any given time. The oxygen atoms are displaced from the ideal 8*c* Wyckoff position to 96*i*. To maintain the stoichiometry, only six oxygen anions are present in each $1\times1\times1$ sub-unit; there are also two vacancies per sub-unit.

Table 1
Space group parameters of superstructure of δ-Bi_2O_3 [5] determined from density functional calculations under the GGA-PAW approximation.

Space group $Fm\bar{3}$, 202					
Unit cell	$a=11.19761$ Å	Volume = 1404.0283 Å^3			
Atom	Wyckoff position	x	y	z	Occupancy
Bi(1)	4*a*	0.0000	0.0000	0.0000	1.00
Bi(2)	4*b*	0.5000	0.0000	0.0000	1.00
Bi(3)	48*h*	0.2500	0.2229	0.0000	0.50
O(1)	96*i*	0.1279	0.0962	0.1460	0.25
O(2)	96*i*	0.4038	0.1460	0.1279	0.25

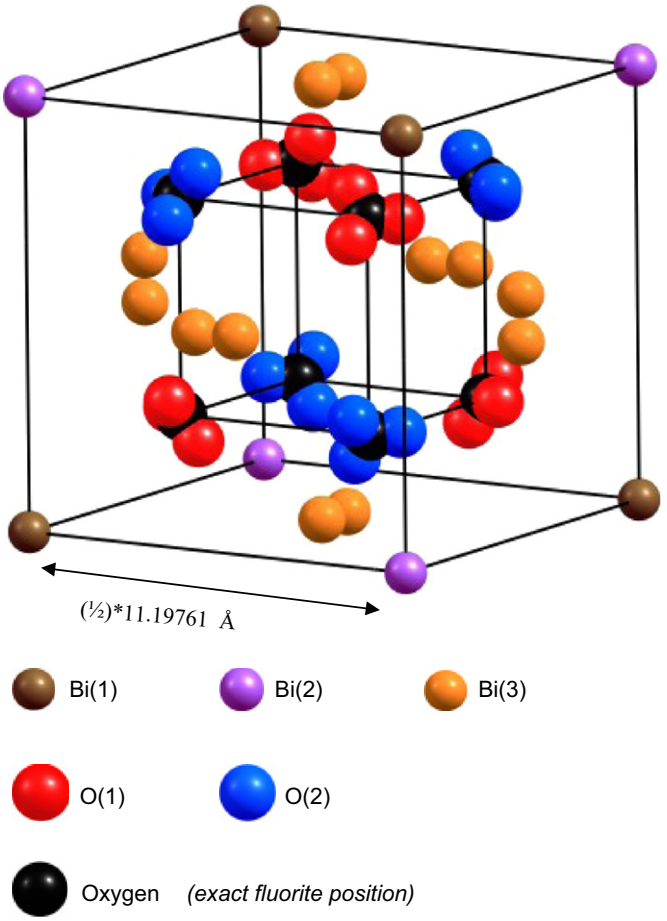

Fig. 1. Crystallographic sites of the space group $Fm\bar{3}$ (202). 1/8 of the $2\times2\times2$ superstructure is shown here. Bi(1) and Bi(2) have an occupancy of 1.0. The Bi(3) sites have an occupancy of 0.5 with only one of the two of nearby available Bi(3) sites being filled at any given time. In the oxygen sub-lattice, for every oxygen fluorite position (black) there are three possible oxygen positions, only one of which is filled either by O(1) or O(2).

The presence of different Wyckoff positions for the same ionic species is due to the differing displacements from the positions that ions would have in the fluorite structure. These displacements arise to accommodate the crystallochemical imbalance resulting from the unoccupied sites (vacancies). Further, since the vacancies are ordered, these displacements are also arranged in an ordered manner. In the following sections, we characterize the relationship between the vacancy ordering on the one hand and the bond lengths, unit cell variation, and the resulting charge on each species on the other.

3.2. Bond lengths

In this section, we will begin by presenting the bond lengths predicted by DFT and then compare them with the estimates from the other, more approximate, method. We will also present the relationship between the different bond lengths and the vacancy ordering.

3.2.1. Bond lengths from DFT calculations

As discussed in the Introduction, the structure of δ-Bi_2O_3 combines vacancy ordering in $\langle 110 \rangle$ and $\langle 111 \rangle$ directions. To characterize the bonding in the structure, it is useful to first examine the structure from the perspective of the Bi ions. The Bi ions are in an octahedral environment with respect to the oxygen-vacancy cubic sub-lattice, i.e., the Bi ions are at the centers of O ion cubes. In the combined vacancy-ordered structure, the Bi ions sit in two different environments [5]: the Bi(1) and Bi(2) ions have vacancy neighbors in the $\langle 111 \rangle$ directions (Fig. 2), while the Bi(3) ions have vacancy neighbors in the $\langle 110 \rangle$ directions (Fig. 3).

3.2.1.1. Cation displacements in the $\langle 111 \rangle$ vacancy ordered oxygen sub-lattices. For the $\langle 111 \rangle$ vacancy ordered oxygen sub-lattice, each Bi(1) and Bi(2) ion is surrounded by six O(1) and O(2) ions, respectively (Fig. 2). As shown in Table 2, all the Bi(1)–O(1) and Bi(2)–O(2) bond lengths are identical. Moreover, as discussed previously, this uniformity in bond lengths is reflected in the electronic degrees of freedom, with the charges between Bi(1)–O(1) and Bi(2)–O(2) being equally distributed [5]. This equivalence in the positions of the oxygen ions ensures that the Bi(1) and Bi(2) ions do not move from their crystallographic sites at the center of the cube. Furthermore, all nearest neighbor O–O separations are 3.138 Å. However, the equal Bi–O bond lengths do not ensure a perfect-cubic (angles = 90°) oxygen sub-lattice. Rather, all the O–O–O angles in the sub-lattice are 72.276°, a very significant deviation from cubic.

3.2.1.2. Cation displacements in the $\langle 110 \rangle$ vacancy ordered oxygen sub-lattice. The oxygen ions in the $\langle 110 \rangle$ vacancy ordered sub-lattice are not all in crystallographically equivalent positions. In this sub-lattice, of the six oxygen ions surrounding each Bi(3), three are in O(1) sites and three in O(2) sites. As a result, the $\langle 110 \rangle$ oxygen sub-lattice is heavily distorted and has three different Bi–O bond lengths (see Table 2). One of the 12 possible $\langle 110 \rangle$ vacancy ordered oxygen sub-lattices is shown in Fig. 3a. In this sub-lattice, there are three O(1) ions, marked as O(1) 1, O(1) 3 and O(1) 6 and three O(2) ions, marked as O(2) 2, O(2) 4 and O(2) 5. There are three different Bi–O bond lengths that occur in pairs; each pair contains two crystallographically different oxygen ions. In Fig. 3a, the Bi(3)–O(1) 6 and Bi(3)–O(2) 5 bond lengths are 2.303 Å. Similarly, the Bi(3)–O(1) 1 and Bi(3)–O(2) 2 bond lengths are 2.399 Å, while the Bi(3)–O(1) 3 and Bi(3)–O(2) 4 bond lengths are 2.559 Å. A consequence of the non-equivalence of the oxygen ions and $\langle 110 \rangle$ vacancy ordering is that the central Bi(3) ion is displaced from its ideal positions (shown by dotted arrow in Fig. 3a) by 0.3036 Å in one of the $\langle 100 \rangle$ directions away from the face of the distorted cube containing the vacancies. In contrast to the simpler geometry of the $\langle 111 \rangle$ oxygen sub-lattice, the $\langle 110 \rangle$ sub-lattice is heavily distorted with these differing bond lengths also resulting in dissimilar O–O–O angles (Fig. 3b).

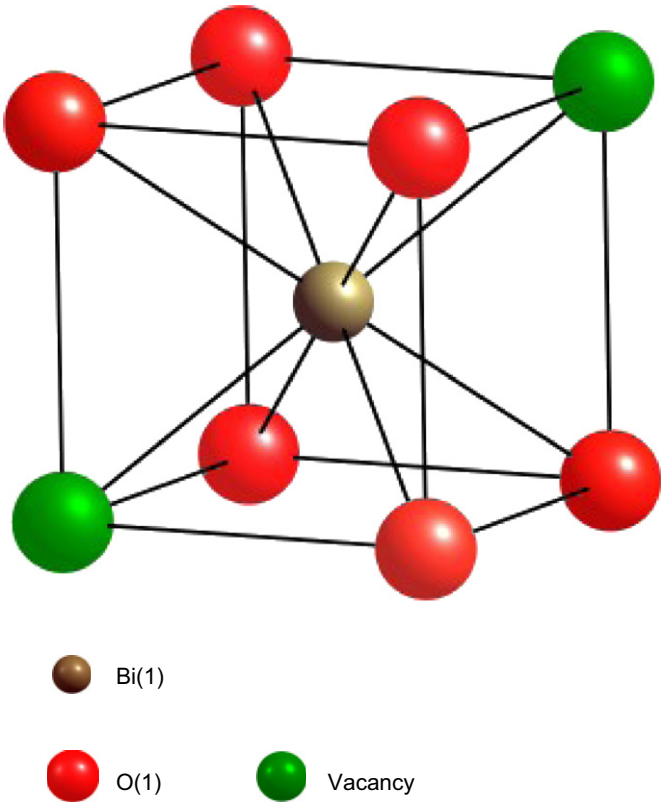

Fig. 2. $\langle 111 \rangle$ vacancy ordered oxygen sub-lattice. Bi(1) present inside the O(1) sub-lattice. All Bi–O bond lengths are 2.426 Å, all O–O distances are 3.138 Å and all O–O–O angles are 72.276°. Similarly, Bi(2) is present inside O(2) oxygen sub-lattice and the sub-lattice has the same geometry.

3.2.1.3. Anion displacement. The DFT calculations show a preferential-directional displacement of all of the oxygen ions. The structural analysis shows that every oxygen ion displaces in the direction of the two first nearest vacancies ordered in $\langle 110 \rangle$, as shown by the solid arrows in Fig. 3a. These two vacancies provide considerable open space in the structure, into which the ions can relax. The result is that both oxygen ions displace from the fluorite site by a magnitude of $x = 0.235$ Å, $y = 0.322$ Å and $z = 0.033$ Å, resulting in a total displacement of 0.4 Å in a direction close to, but not exactly parallel to $\langle 110 \rangle$.

3.2.2. Bond lengths from Shannon radii

There are several standard ways to estimate the bond lengths in ionic materials, including analysis of the Shannon radii [13]. In this sub-section section we assess the value of Shannon radii method for analyzing Bi_2O_3.

The bond lengths calculated from the radii given by Shannon [13] are based on the coordination environment. In ideal structures without defects, the bond lengths predicted by Shannon radii are quite accurate [13]. However, in the presence of defects or vacant lattice sites, as in the δ-Bi_2O_3 structure, the bond lengths can either deviate from the expected values or sometimes can provide only incomplete information, as we find to be the case in the following analysis.

Every cation in an ideal fluorite structure is coordinated with eight anions. However, in δ-Bi_2O_3, each Bi^{3+} ion is coordinated with only six oxygen ions, the other two anion sites being vacant. According to the Shannon radii [13], $r_{Bi^{3+}}(VI) = 1.03$ Å, $r_{Bi^{3+}}(VIII) = 1.17$ Å and $r_{O^{2-}}(IV) = 1.38$ Å. This yields estimates of the Bi(VI)–O of 2.41 Å. This estimated bond length is actually very close to the Bi–O bond length of 2.424 Å in the non-distorted $\langle 111 \rangle$ ordered oxygen sub-lattice. Interestingly, although six coordinated, the DFT calculations yield Bi–O bond lengths in the $\langle 110 \rangle$ sub lattice as 2.559 Å, which is very close to the Bi(VIII)–O bond length of 2.55 Å. Hence, in this case the Shannon radii predictions are in close agreement with some Bi–O bond lengths given by DFT, but not others.

3.3. Sub-unit cell distortion

Thus far, we have characterized that ionic displacements of both Bi and O ions from their ideal fluorite positions are induced by the vacancies in δ-Bi_2O_3. As a consequence, the structure is distorted locally. In this section, we characterize these local

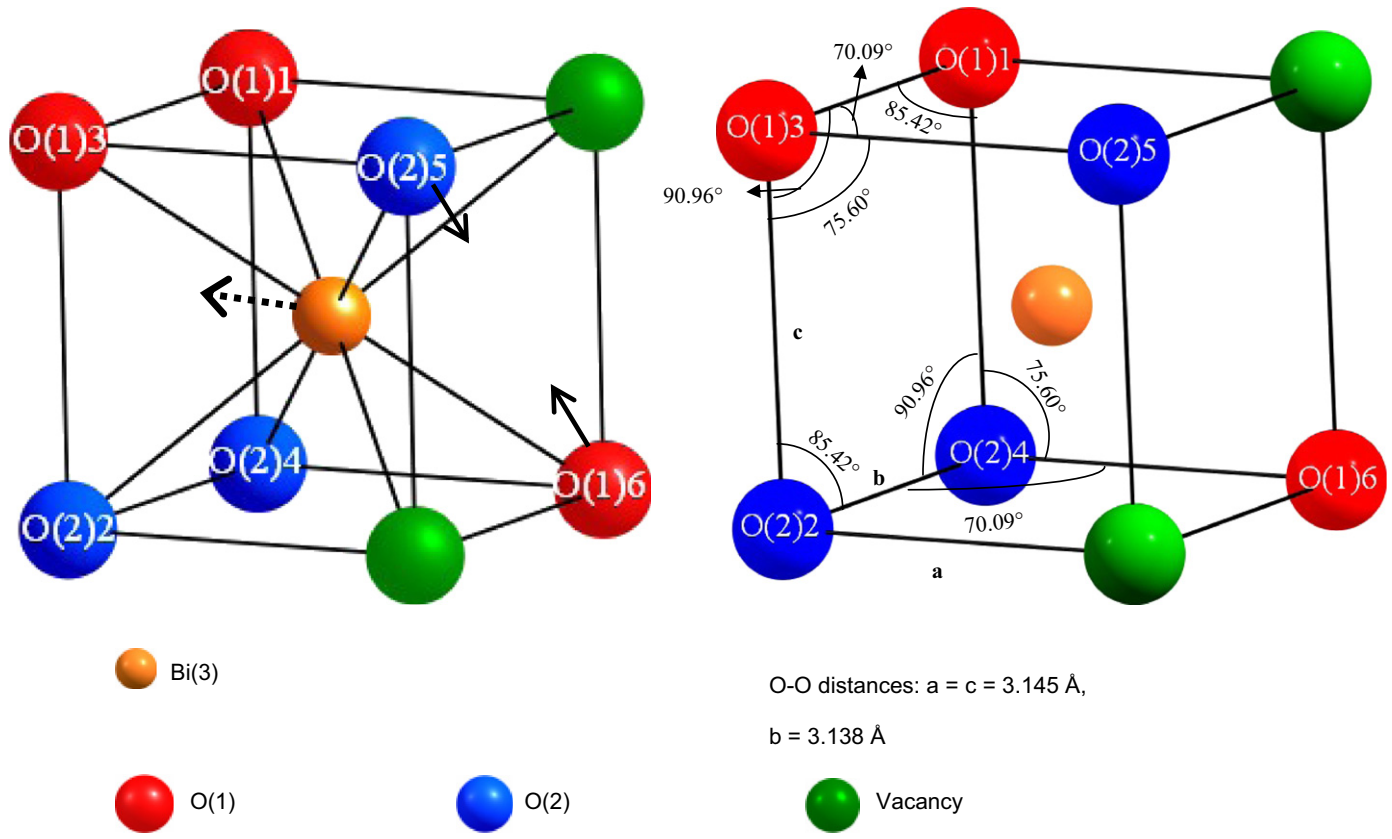

Fig. 3. ⟨110⟩ Vacancy-ordered oxygen sub-lattice: (a) Bi(3) present inside the oxygen sub-lattice formed by three O(1), three O(2) and two vacancies. There are three different pairs of Bi–O bond lengths: Bi(3)–O(1)6 and Bi(3)–O(2)5 = 2.303 Å, Bi(3)–O(1)1 and Bi(3)–O(2)2 = 2.399 Å, Bi(3)–O(1)3 and Bi(3)–O(2)4 = 2.559 Å. The dotted arrow shows Bi(3) displacement in ⟨100⟩ direction by 0.3036 Å away from the plane containing the vacancies and solid arrows on O(2)5 and O(1)6 show the oxygen displacement in a direction close to ⟨110⟩ and (b) schematic showing the geometrical values of the distorted ⟨110⟩ oxygen sub-lattice. Only O–O distances and O–O–O angles are shown; those involving a vacancy are not shown.

Table 2
Bi–O bond lengths in the ⟨110⟩ and ⟨111⟩ vacancy ordered sub-lattice.

	⟨111⟩	Å
Bi(1)–O	O(1)	2.426
Bi(2)–O	O(2)	2.426
	⟨110⟩	
Bi(3)–O	O(1) 5, O(2) 6	2.303
	O(1) 1, O(2) 2	2.399
	O(1) 3, O(2) 4	2.559

The two ⟨111⟩ vacancy ordered sub-lattices has Bi(1) and Bi(2) ions surrounded by six O(1) and six O(2) ions, respectively. The ⟨110⟩ vacancy ordered sub-lattice has three O(1) and three O(2) ions surrounding each Bi(3) ion.

distortions from the perspective of the FCC network of Bi ions. As Fig. 4(a) shows, the Bi network can be considered either as an FCC network with Bi(1) and Bi(2) ions in the eight corners and Bi(3) ions of the six phases, or as a network with Bi(3) ions at the eight corners and on four of the six faces, the remaining two faces being occupied by a Bi(1) and a Bi(2) ion. These two distinct, interpenetrating FCC networks are shown in Fig. 4a. The difference between the two networks can be characterized by the shape of the boxes defined by the corner Bi ions. Recalling that the Bi(1) and Bi(2) ions sit at the standard fluorite sites, see Table 1, the box defined by these ions, Fig. 4b, is a perfect cube with the Bi–Bi second nearest neighbor distance being half the lattice parameter, 5.5988 Å. By contrast, the FCC network defined by the Bi(3) ions in the corners, which are displaced by 0.3036 Å along ⟨100⟩ as shown in Fig. 4c is distorted. In Fig. 4c, the Bi–Bi distance between ions 2 and 20 and between ions 4 and 21 is not affected by the displacement and remains 5.5988 Å, as is in the undistorted Bi(1)–Bi(2) FCC sublattice. However, the anti-parallel displacement of the columns of ions has the consequence that the distance between ions 2 and 4, and between ions 20 and 21 ions increases to 5.6316 Å. (Similar anti-parallel displacements occur between ions 2 and 15 and between ions 20 and 18.) These displacements distort the box such that while α remains 90° β and γ deviate significantly, taking the value of 96.18°. Each $2\times2\times2$ superstructure contains an equal number of these distorted FCC networks oriented along crystallographic axis. Thus, despite these distortions, due to the anti-parallel displacements in all three crystallographic axis, the overall system is cubic.

In the distorted FCC network, 12 of the 14 cations are Bi(3) ions with the remaining two being either Bi(1) or Bi(2). Depending on the choice of the Bi(3) FCC network, both of the non-displaced ions could be at their Wyckoff positions or one could be in a Bi(1) site and the other in Bi(2) site. In the non-distorted FCC network (Fig. 4b), 8 out of the 14 Bi FCC ions are non-displaced, i.e., four each from Bi(1) and Bi(2); the remaining six are Bi(3).

Battle et al. [14] also postulated a similar kind of FCC network to the non-distorted network that we have presented. In the Y_2O_3–Bi_2O_3 system, they expected Bi^{3+} to occupy all Bi(3) positions (as we also see), whereas, the rest of the positions at the corners of the unit cell (see Fig. 4a) could be occupied either of

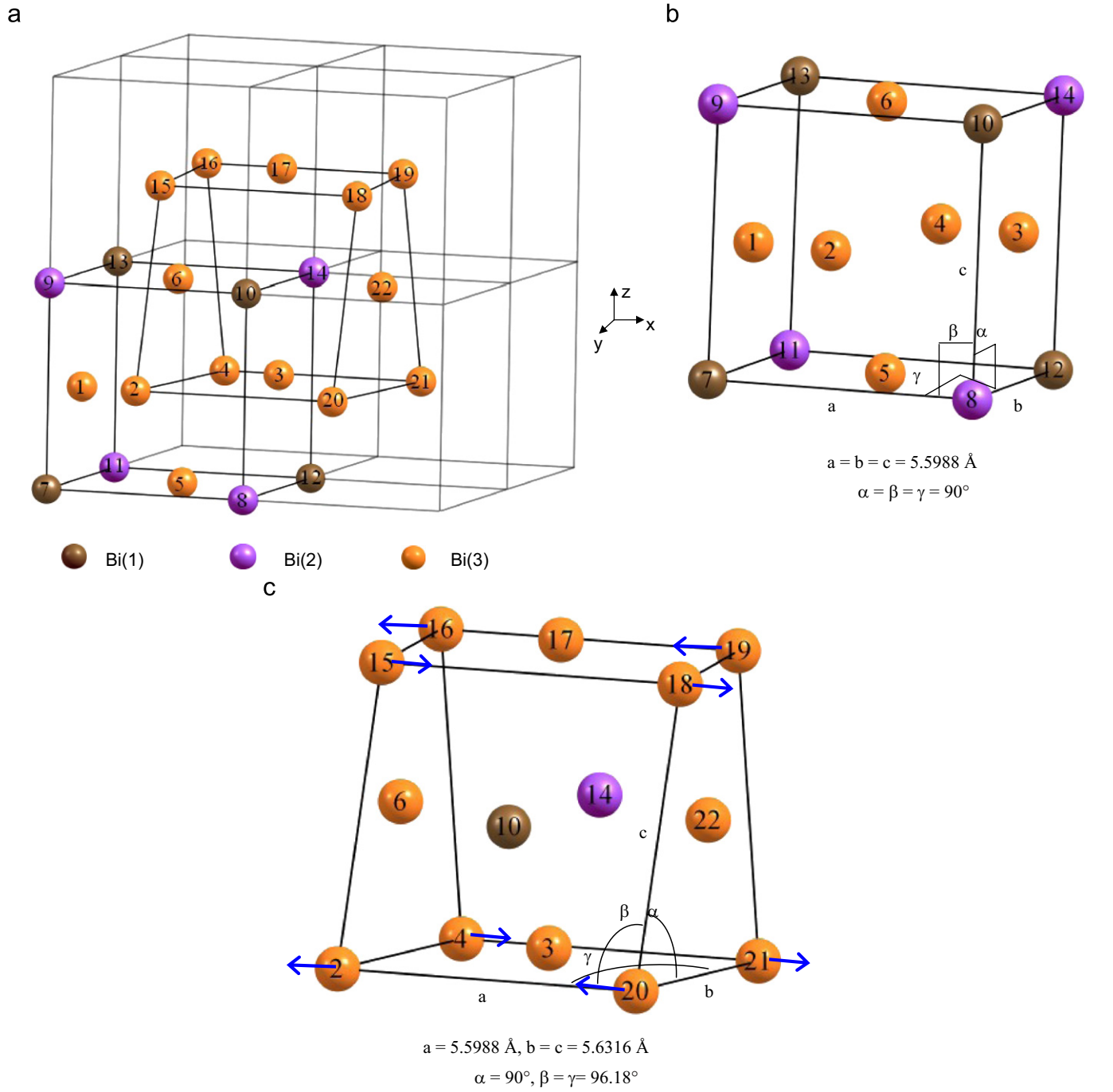

Fig. 4. (a) Schematic of two interpenetrating FCC networks in $2 \times 2 \times 2$ superstructure. (b) A non-distorted cubic FCC network formed by four Bi(1), four Bi(2) and six Bi(3) cations. (c) A distorted FCC network formed by 12 Bi(3); the other two cations can be either both of same Wyckoff number or different (Bi(1), Bi(2)). The corners of the non-distorted FCC network are formed by Bi(1) and Bi(2) whereas those of distorted FCC network are formed by Bi(3) cations. For clarity, oxygen ions are not shown.

Y^{3+} and Bi^{3+}. In their analysis, they did not, however, distinguish between the non-distorted and the distorted networks.

4. Electronic structure of vacancy-ordered δ-Bi_2O_3

We have shown above that there are two different vacancy-ordered environments around the Bi ions. As a result the crystallographically different Bi ions have different Bi–O bond lengths. While we have discussed the Bi–O bonds from the structural viewpoint, it is also instructive to analyze them from the charge distribution perspective. The ionicity of the ions and the surrounding atomic environment affects the bond length. In this section, we show the effect of the vacancy ordering on the ionicity (charge distribution) of the ions and the bond lengths.

We have characterized the charge distributions associated with the Bi and O ions using Bader charge analysis [15,16] of the electronic structure determined from DFT. Table 3 shows the charges categorized on the basis of the Wyckoff position. If Bi_2O_3 were fully ionic, the Bi and O ions would have formal charges of +3e and −2e, respectively. Instead, Bader charge analysis shows that the Bi(1) and Bi(2) have a DFT atomic charge of +2.1232e while the Bi(3) ions have a charge of +2.8411e. These differences from the formal charge indicate the degree of covalency.

Table 3
Electronic charge on the ionic species based on their Wyckoff position.

Atom	Wyckoff position	Charge (e)
Bi(1)	4*a*	2.1232
Bi(2)	4*b*	2.1232
Bi(3)	48*h*	2.8411
O(1)	96*i*	−1.7751
O(2)	96*i*	−1.7737

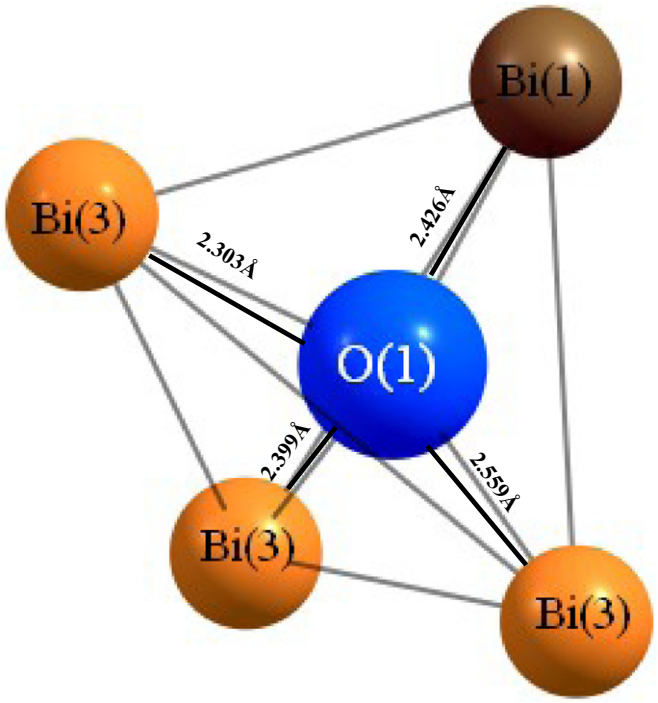

Fig. 5. Bismuth tetrahedral formed by three displaced Bi(3) and one displaced with an oxygen in the center. The Bi(1) and O(1) are shown here. A similar arrangement is also applicable to Bi(2) and O(2).

The charge on the O ions is −1.77e, and is independent of the Wyckoff position. Numerically, the deviation of the DFT atomic charge from the formal charge gives the amount of charge associated with covalent bonding.

It is useful to characterize the charge distribution from the perspective of the Bi tetrahedra (Fig. 5). Irrespective of the kind of oxygen, O(1) or O(2), present inside the tetrahedron, three of the four Bi ions are of higher ionic charge +2.84 e Bi(3) ions, and one is either a Bi(1) or Bi(2), and has charge +2.12e. Moreover, all four Bi–O bonds inside the tetrahedra have different lengths. The tetrahedral configuration of Bi ions is same even around the vacancies.

5. Comparison with bixbyite structure

The bixbyite structure displays $Ia\bar{3}$ space group symmetry with a cell formula $M_{32}O_{48}$ consisting of 32 cations, 48 anions and 16 vacant anion sites. The cations occupy 8*a* and 24*d* sites at 0, 0, 0 and *x*, 0, 0.25, respectively, and the anions occupy 48*e* sites at *x*, *y*, *z*. It is interesting to notice that while the vacancy-ordered structure of δ-Bi_2O_3 very closely resembles that of the bixbyite structure, it is actually distinct.

On the one hand, the vacancies and the cations have similar crystallographic positions and the vacancies have same site occupancy in both the structures, thus, resulting in the same ordering of vacancies. Using coordination defect theory, Bevan and Martin [17] have recently shown 3D vacancy networks in ⟨110⟩ directions in bixbyite Mn_2O_3. These vacancy networks are connected by ⟨111⟩ vacancy linkages. This is identical to the ⟨110⟩–⟨111⟩ vacancy in Bi_2O_3 [5,18]. The cations show similar crystallographic characteristics in both the structures. In particular, in each structure there are eight non-displaced and 24 displaced cations. Further, the vacancy environment around two different cations remains the same (Figs. 2 and 3).

On the other hand, the anion positions in the two structures are different, arising from different displacements relative to the cation positions. To elucidate these differences, we performed a DFT simulation starting with Bi_2O_3 arranged in the bixbyite structure. During the relaxation, the O ions move considerably; the final structure is that originally obtained structure for δ-Bi_2O_3 with space group symmetry $Fm\bar{3}$ as previously reported [5]. It is quite possible that the differences in the anion sublattice, responsible for the difference between the two structures, arises from the lone pair electrons of Bi, that are absent in other cations crystallizing in bixbyite structures.

6. Relation to experiment

We first address the issue of the overall nature of the defect ordering. Our earlier MD simulations showed that the high polarizability of Bi ions leads to continuous diffusion in the system. As a result the combined ⟨110⟩–⟨111⟩-ordered defect structure does not become locked in. Our simulations further showed that the presence of unpolarizable or weakly polarizable cations does result in the ordered defect structure being produced, and that it has a structure that is consistent with that found in the experimental analysis of doped Bi_2O_3 by Wachsman et al. [18]. It is this structure that we have analyzed in this paper and it can be considered as the prototype for the structure present in the doped system. It is thus appropriate to place our crystallographic analysis in the context of the experimental results for doped systems.

Anion displacement and vacancy ordering in δ-Bi_2O_3 has long been a subject of discussion, with several contradictory models being presented [14,19–23]. A detailed discussion of these models can be found in Boyapati et al. [24] Here we only address the issue of the anion displacement within the defect ordered structure. Based on neutron-diffraction data, Willis et al. [22] presented an oxygen sub-lattice model (anion cubic sub-lattice) in which all the anions were suggested to be displaced in ⟨111⟩ directions, i.e., a displacement from regular tetrahedral site, 8*c* $(\frac{1}{4},\frac{1}{4},\frac{1}{4})$, to an interstitial site, 32f (0.3,0.3,0.3). Battle et al. [25] suggested a similar displacement in pure Bi_2O_3. In Y_2O_3–Bi_2O_3 [19], however, they found that a higher concentration of yttria decreased the concentration of ⟨111⟩ displaced anions, with some evidence of ⟨110⟩ anion displacement. By contrast, the experiments by Boyapati et al. have, however, found that in the doped Bi_2O_3, anion displacement occurs in ⟨111⟩ directions; they did not observe any signature of ⟨110⟩ displacement. An increased concentration of less polarizable dopants (Y^{3+} compared to Dy^{3+}) increases the number of ⟨111⟩ displaced anions. As Boyapati et al. [24] point out, the difference between their results and those of Battle et al. may be due to the fact that their samples were not aged while those of Battle et al. were aged. DFT calculations also reveal anion displacement that are close to but not exactly along ⟨110⟩, and our observations are thus are to a large extent consistent with the results of Battle et al. [14,19].

We now return to pure δ-Bi_2O_3. The actual defect structure of δ-Bi_2O_3, which is only stable at high temperature, has

not been fully characterized. While it is possible that this structure, evolving through diffusion, is not related to the ordered structure inherent to the doped systems, it also seems reasonable that at any single instant in time for any small region of the crystal, the structure would strongly resemble one the crystallographically equivalent variants of the defect-ordered structure. Further structural characterization and simulation are required to resolve this issue.

Finally, we address the issue as to the conditions under which the vacancy-order structure can be formed. As discussed in the Introduction, once a combined vacancy-ordered structure is formed, the structure locks the oxygen and the vacancies to their respective positions limiting any oxygen diffusion. It appears that the electronic charge distribution plays a significant role in limiting the diffusion. Since a covalent bond is directional and difficult to break, we speculate that the Bi(3)–O bond is the limiting factor in the oxygen diffusion in the vacancy ordered system. As such, it is anticipated that variations in the Bi(3)–O bond characteristics might be the key crystallo-chemical variable chiefly responsible for tailoring the ionic conductivity of bismuth oxide based electrolytes. A corresponding argument may well be applicable to ZrO_2 and CeO_2 based electrolyte materials.

6. Conclusions

Taken together, due to atomic displacements as a result of ordering of the vacant crystallographic sites, our DFT calculations show that the crystal structure of δ-Bi_2O_3 is a $2\times2\times2$ fluorite super-structure. It has a lower symmetry, $Fm\bar{3}$, compared to $Fm\bar{3}m$ of the regular fluorite structure. Based on the directionality of vacancy ordering, the cations are either displaced or non-displaced. Furthermore, the electronic charge of the cations is affected by the vacancy ordering. By contrast, the anions are found to be un-affected by the vacancy ordering. Bader charge analysis illustrates that the presence of some covalent-bond character in Bi(3)–O which affects lowering of oxygen diffusivity. We leave for future work, similar modeling of the multi-component system to understand the effects of the dopants in δ-Bi_2O_3.

Acknowledgments

This work was supported by NASA under Grant NAG3–2930 and by DOE through the High Temperature Electrochemistry Center (HiTEC) at the University of Florida, Contract no. DE-AC05-76RL01830. JCN also acknowledges the financial support by the US National Science Foundation (CBET-0730900). We are happy to acknowledge the University of Florida High-Performance Computing Center for providing computational resources and support that have contributed significantly to the research results reported in the paper. The authors would also like to thank Lu Cai for her assistance with the polyhedra distortion analysis.

References

[1] N. Jiang, E.D. Wachsman, S.H. Jung, Solid State Ionics 150 (2002) 347.
[2] T. Takahashi, H. Iwahara, Materials Research Bulletin 13 (1978) 1447.
[3] N. Jiang, E.D. Wachsman, Journal of American Ceramic Society 82 (1999) 3057.
[4] E.D. Wachsman, S. Boyapati, N. Jiang, Ionics (2001) 1.
[5] D.S. Aidhy, J.C. Nino, S.B. Sinnott, E.D. Wachsman, S.R. Phillpot, Journal of American Ceramic Society 91 (2008) 2349.
[6] G. Kreese, J. Hafner, Physical Review B 49 (1994) 14251.
[7] G. Kreese, J. Furthmuller, Physical Review B 54 (1996) 11169.
[8] G. Kreese, J. Furthmuller, Computational Materials Science 6 (1996) 15.
[9] J.P. Perdew, Y. Wang, Physical Review B 45 (1992) 13244.
[10] P.E. Blochl, Physical Review B 50 (1994) 17953.
[11] H.A. Harwig, A.G. Gerards, Thermochemica Acta 28 (1979) 121.
[12] T. Hahn, International Tables of Crystallography, vol. A, fifth ed., Kluwer Academic Publishers, Boston, 2002.
[13] R.D. Shannon, Acta Crystallographica Section A 32 (1976) 751.
[14] P.D. Battle, C.R.A. Catlow, L.M. Moroney, Journal of Solid State Chemistry 67 (1987) 42.
[15] G. Henkelman, A. Arnaldsson, H. Jonsson, Computational Materials Science 36 (2006) 254.
[16] E. Sanville, S.D. Kenny, R. Smith, G. Henkelman, Journal of Computational Chemistry 28 (2007) 899.
[17] D.J.M. Bevan, R.L. Martin, R. Smith, G. Henkelman, Journal of Solid State Chemistry 181 (2008) 2250.
[18] E.D. Wachsman, S. Boyapati, M.J. Kauffman, N. Jiang, Journal of American Ceramic Society 83 (2000) 1964.
[19] P.D. Battle, C.R.A. Catlow, J.W. Heap, L.M. Moroney, Journal of Solid State Chemistry 63 (1986) 8.
[20] G. Gattow, H. Schroder, Zeitschrift Fur Anorganische Und Allgemeine Chemie 318 (1962) 176.
[21] L.G. Sillen, Ark Kemi Mineral Goelogy 12A (1937) 1.
[22] B.T.M. Willis, Acta Crystallographica 18 (1965) 75.
[23] P.W.M. Jacobs, D.A. MacDonaill, Solid State Ionics 23 (1987) 279.
[24] S. Boyapati, E.D. Wachsman, N. Jiang, Solid State Ionics 140 (2001) 149.
[25] P.D. Battle, C.R.A. Catlow, J. Drennan, A.D. Murray, Journal of Physics C: Solid State Physics (1983) L561.